REPORT

ULTRACOLD CHEMISTRY

Imaging the onset of the resonance regime in low-energy NO-He collisions

Tim de Jongh[1]*, Matthieu Besemer[1]*, Quan Shuai[1]*, Tijs Karman[2], Ad van der Avoird[1], Gerrit C. Groenenboom[1]†, Sebastiaan Y. T. van de Meerakker[1]†

At low energies, the quantum wave–like nature of molecular interactions results in distinctive scattering behavior, ranging from the universal Wigner laws near 0 kelvin to the occurrence of scattering resonances at higher energies. It has proven challenging to experimentally probe the individual waves underlying these phenomena. We report measurements of state-to-state integral and differential cross sections for inelastic NO-He collisions in the 0.2 to 8.5 centimeter^{-1} range with 0.02 centimeter^{-1} resolution. We studied the onset of the resonance regime by probing the lowest-lying resonance dominated by *s* and *p* waves only. The highly structured differential cross sections directly reflect the increasing number of contributing waves as the energy is increased. Only with CCSDT(Q) level of theory was it possible to reproduce our measurements.

The study of collisions between atoms and molecules at the full quantum level has been an important research goal in chemistry and physics for decades (*1*). To date, the internal rotational and vibrational states of molecules have received the most attention, and a rich variety of experimental methods has been developed to select a single quantum state before the collision and to probe the occupied quantum states of the products (*2*). The wealth of experimental and theoretical state-to-state scattering studies has contributed immensely to our present understanding of molecular interactions (*3*).

Yet in addition to these internal states, the angular momentum associated with the relative motion of the particles is also quantized. It is described by a set of orbital angular momentum states, or partial waves, with integer quantum number ℓ, which takes the values $\ell = 0, 1, 2, \ldots$ with names *s*, *p*, *d*, ...-wave, respectively. The contribution of each partial wave to a scattering cross section describes how the reagents transform into products at the most fundamental state-to-state level and contains all of the information about the scattering event.

The influence of a single partial wave to a collision event is in principle directly encoded in the differential cross sections (DCSs), which can be probed experimentally. For atom-atom collisions, each wave will result in a distinctive angular distribution in which the number of nodes observed in a DCS equals the value of ℓ (*4*). That is, *s*-wave scattering leads to an isotropic DCS, *p*-wave scattering results in a single node, and so on. For molecular systems with anisotropic interactions, multiple partial waves contribute and interfere with each other, resulting in a more complicated DCS pattern from which the partial wave composition cannot be directly discerned. The identification of the partial wave composition of a collision event from experimental observations has therefore remained a formidable challenge (*5*), preventing state-to-state experiments at the full partial-wave level.

The effects of individual partial waves may best be observed in situations in which only a limited number of interfering waves contribute. This number critically depends on the particles' de Broglie wavelengths and, hence, the collision energy (*6*, *7*). If the energy is too high, a large number of waves contribute, so that the collisions may be regarded as semiclassical, and the dynamics can often be described with semiclassical models. There is no hope to disentangle the contribution of individual waves from experimental observations in this regime. By contrast, at energies approaching 0 K, only the lowest allowed partial wave (for most systems, this is the *s*-wave) contributes, leading to universal rules for the energy dependence of collision cross sections in the form of Wigner's threshold laws (*8*). In this "ultracold" regime, the *s*-wave results in DCSs that contain no intrinsic structure; the number of contributing waves is too low to harness information on the interaction potential and collision dynamics from state-to-state experiments.

As the energy is increased from the ultracold limit, the number of contributing partial waves consecutively increases, yielding unprecendented opportunities to directly observe the effect of individual waves on the scattering cross section. The regime is entered where scattering resonances occur in the collision cross sections: When the collision energy becomes resonant with a quasi-bound state supported by the interaction potential, the incident particles are temporarily captured into a quasi-bound long-lived complex (*9*). In a simplified picture, these resonances may be regarded as the orbiting of the atom around the molecule (a shape resonance) or as the transient excitation of the molecule to a state of higher energy (Feshbach resonance). Analogous to Bohr's model of electrons orbiting around an atom's nucleus with given angular momentum, the atom-molecule binary system is stabilized when the collision energy is resonant with a partial wave that fits on the atom's orbit an integer number of times. The corresponding "resonant" partial wave will dominate the scattering process, which appears as a sudden increase in the integral cross section (ICS) at the resonance energy. The resonant wave will dominate the DCS as well, resulting in an angular distribution that fits the value for ℓ from which the resonance originates. Measurements of DCSs at resonances therefore yield the distinctive opportunity to experimentally probe the partial-wave fingerprint of the collision process, revealing the scattering mechanism at the most fundamental state-to-state quantum mechanical level.

Scattering resonances are extremely sensitive to the details of the potential energy surface (PES), in particular at energies just above the ultracold Wigner limit at which only a few waves with $\ell > 0$ start contributing. Their observation has been a quest in molecular physics for decades (*10*); however, it has proven extremely challenging to experimentally reach the low energies to access the relevant energy region and the high-energy resolutions required to scan the energy over the resonances and to probe DCSs (*11*–*15*). In ultracold gases, scattering resonances are routinely induced by tuning external fields to shift bound states into resonance (*16*, *17*), but *s*-wave collisions observed in such experiments invariably result in isotropic DCSs, containing little information about the collision dynamics. To date, only a few experiments have succeeded in directly measuring the energy dependence of state-to-state cross sections near resonances, mostly by using molecular beam methods (*18*). Resonances in ICSs have been observed by using the crossed-beam approach, using a small beam intersection angle (*19*–*23*). Using merged beams, resonances in Penning ionization cross sections of metastable atoms with atomic and molecular partners have been studied at energies down to 0.01 cm^{-1} (*24*–*28*). Measurements of resonance features in state-to-state DCSs for inelastic collisions have recently also become possible by using the Stark deceleration and velocity map imaging techniques

[1]Institute for Molecules and Materials, Radboud University, 6525 AJ Nijmegen, Netherlands. [2]Institute for Theoretical Atomic Molecular and Optical Physics, Center For Astrophysics, Harvard and Smithsonian, Cambridge, MA 02138, USA.
*These authors contributed equally to this work.
†Corresponding author. Email: basvdm@science.ru.nl, gerritg@theochem.ru.nl

(*29*, *30*), although the lowest energy achieved was limited to 13 cm^{-1}, which is typically two to three orders of magnitude too hot to probe individual partial waves. Measurements of state-to-state ICSs and DCSs at energies that approach the ultracold Wigner regime, at which only a few waves contribute, have remained elusive, hampering a detailed view on how molecular collisions evolve from the pure quantum single-partial-wave into the multi-partial-wave regime (*31*).

Here, we report the measurement of state-to-state ICSs and DCSs for inelastic collisions between state-selected NO [$X^2\Pi_{1/2}$, $v = 0, j = 1/2f$, hereafter referred to as $(1/2f)$ (*32*)] radicals and He atoms in a crossed-beam experiment at energies between 0.2 and 8.5 cm^{-1}, with an energy resolution of 0.02 cm^{-1}. Three fully resolved partial-wave resonances were observed in the ICS, and the incline of a fourth resonance was observed at the lowest energies. These resonances originated from the lowest-lying quasi-bound states supported by the NO-He interaction potential just above the energetic long-range asymptote. They correspond to values for ℓ that follow a progression from the lowest possible value and probe the onset of the resonance regime at energies connecting to the ultracold Wigner limit. Rapid variations were observed in the highly structured DCSs as the energy was scanned over the resonances, in which the number of nodes observed in the angular distributions directly reflected the increasing value of ℓ as the energy was increased. We found that our measurements of the lowest partial-wave resonances in NO-He could not be reproduced satisfactorily by the most advanced NO-He PES at the CCSD(T) (*33*) level of theory. Good agreement was only obtained with an ab initio PES at the CCSDT(Q) (*33*) level. Such level of precision was previously only needed for high-resolution spectroscopy of bound states probing the PES in the region of the well (*34*) and anticipated for low-energy scattering resonances (*30*). The need for theory at the CCSDT(Q) level as demonstrated here for NO-He collisions illustrates the unprecedented sensitivity of scattering resonances in probing PESs accross their entire energy landscapes.

We used a crossed-molecular-beam apparatus that combines Stark deceleration and velocity map imaging (VMI) (supplementary materials). A packet of NO $(1/2f)$ radicals with a computer-controlled velocity and a narrow velocity spread was produced by using the Stark decelerator. A beam of He atoms was produced with a cryogenic valve held at temperatures between 11 and 18 K. Beam intersection angles of 5° and 10° were used to cover the 0.2 to 3 cm^{-1} and 0.8 to 8.5 cm^{-1} energy ranges, respectively. The collision energy resolution ranged from 0.02 cm^{-1} for the lowest collision energies to 0.7 cm^{-1} for the highest energies. The scattered NO radicals were state-selectively detected by using a two-color laser ionization scheme and velocity mapped on a two-dimensional detector. The measurements with a 5° intersection angle were performed by using a VMI detector that offered improved velocity resolution.

We studied collisions that de-excite the NO radicals from the $(1/2f)$ to the $(1/2e)$ level, which have an energy splitting of 0.01 cm^{-1} (*35*). For ICS measurements, we scanned the collision energy between 0.2 and 8.5 cm^{-1} and observed three prominent resonances in the relative ICS with almost zero scattering probability at energies in between the resonances (Fig. 1A). The incline of a fourth resonance was observed below 1 cm^{-1}. We compared the experimentally obtained relative ICS with theoretical ICSs, convoluted with the experimental resolution, based on two sets of PESs (Fig. 1A

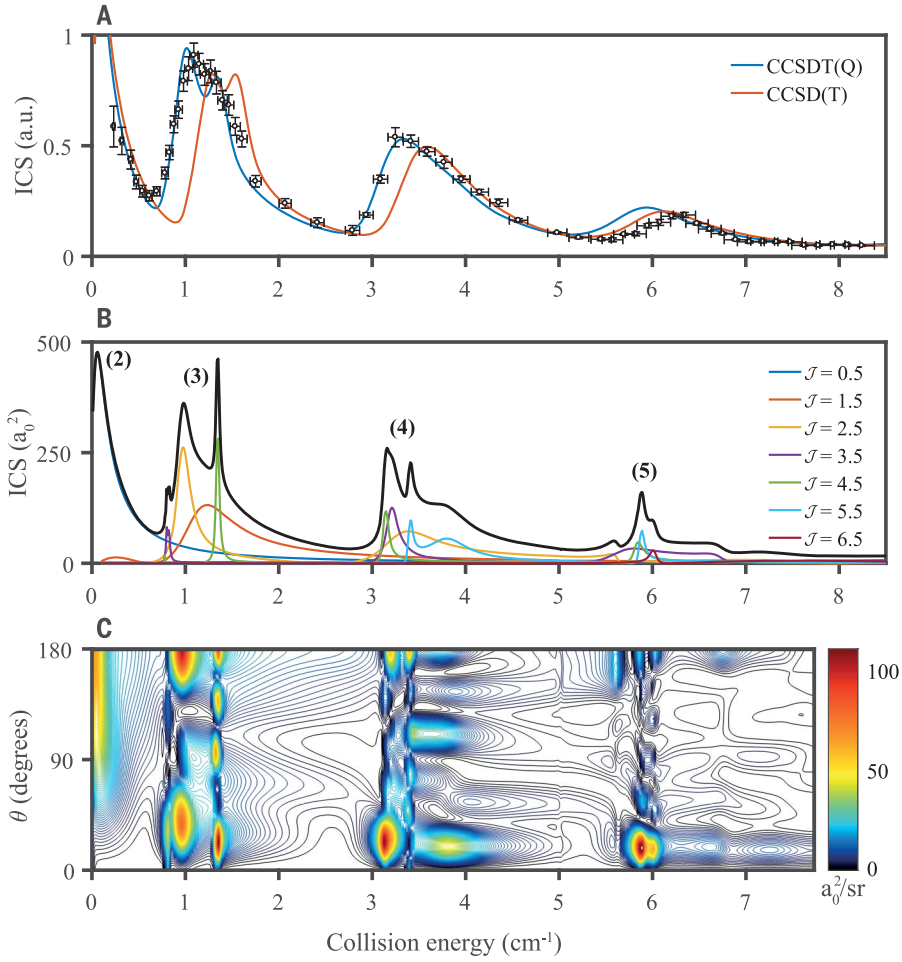

Fig. 1. Collision energy dependence of integral and differential cross sections for inelastic NO-He ($j = 0.5f \rightarrow 0.5e$) collisions. (**A**) Comparison between measured (data points with error bars) and calculated (solid curves) cross sections based on CCSD(T) and CCSDT(Q) potentials. Experimental data are in a.u., arbitrary units. Data were accumulated using a continuous cycle over collision energies. Vertical error bars represent statistical uncertainties at 95% of the confidence interval. Horizontal error bars represent uncertainties in energy calibration. The calculated cross sections were convoluted with the experimental energy resolution. (**B**) Theoretically predicted state-to-state cross section based on the CCSDT(Q) potential (black), together with the contribution of each angular momentum state with quantum number $\mathcal{J}$. The value for the resonant partial wave ℓ_{res} is given in parenthesis. (**C**) Contour plot of theoretically calculated [CCSDT(Q)-potential] DCS as function of collision energy.

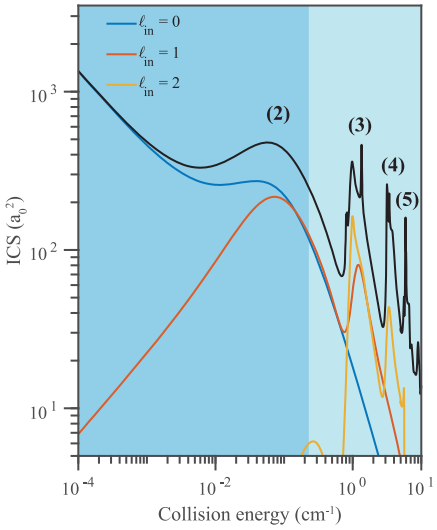

Fig. 2. Logarithmic plot of theoretical ICSs based on the CCSDT(Q)-potential. Included are the contributions of *s*, *p*, and *d* partial waves in the ingoing channel. The value for the resonant partial wave ℓ_{res} is given in parenthesis. The light blue shaded area indicates the energy region probed in our measurements.

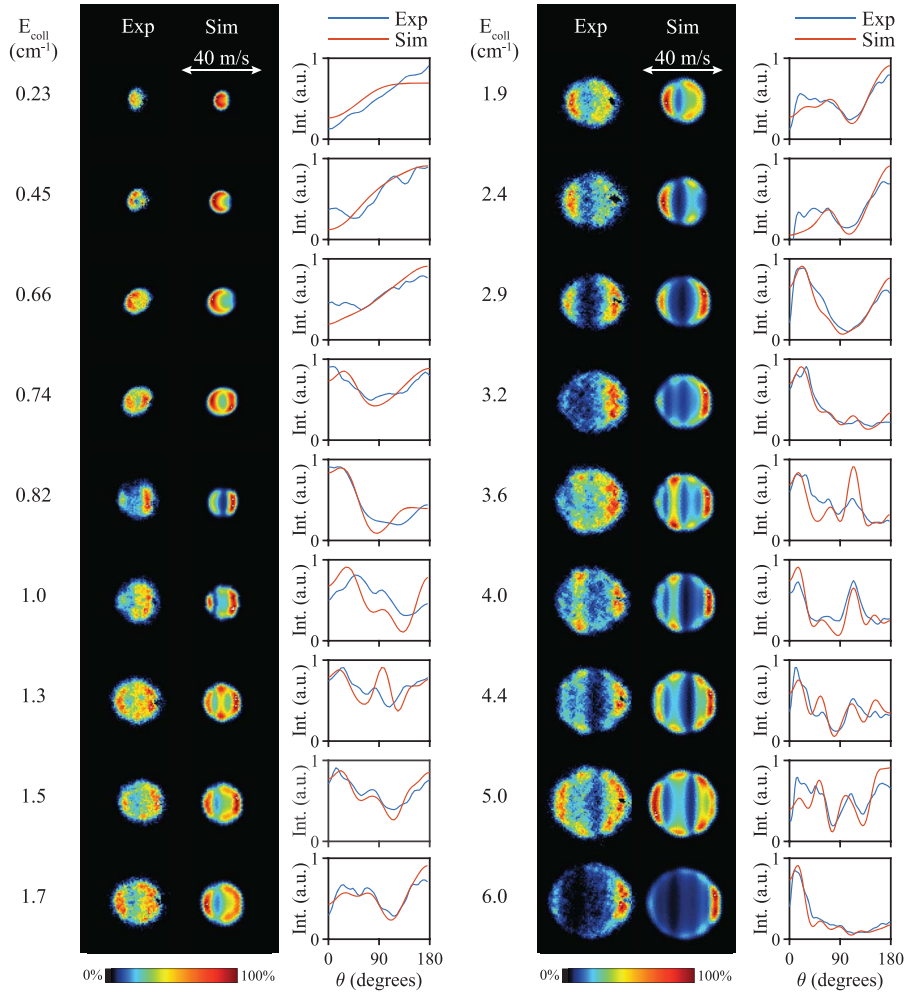

Fig. 3. Experimental and simulated ion images based on the CCSDT(Q) potential at selected collision energies. Exp, experimental; Sim, simulated. The images are presented so that the relative velocity vector is oriented horizontally, with the forward direction on the right side of the image. Small segments of the images around forward scattering are masked owing to imperfect state selection of the NO packet. The angular scattering distributions as derived from the experimental (blue curves) and simulated (red curves) images are shown for each collision energy.

and fig. S6). The first set of potentials was computed at the UCCSD(T)/CBS (*33*) limit by using a complete basis-set extrapolation (CBS) scheme. The second set of PESs were computed at the UCCSDT(Q)/CBS (*33*) level. We refer to the sets as CCSD(T) and CCSDT(Q) potentials, respectively. The CCSDT(Q) potential is deeper than the CCSD(T) potential by about 0.6 cm^{-1} near the well of the potential (table S1) and causes a linear shift of roughly 0.25 cm^{-1} in the position of all the calculated resonances. We found that the CCSDT(Q) corrections were essential to quantitatively describe the lowest-lying resonances, although the resonance observed near 6.5 cm^{-1} was predicted at slightly lower energies by both potentials. We performed several tests to investigate the possible origin of this discrepancy. A few test points computed at the UCCSDTQ(P) (*33*) level suggest that the electron correlation for the UCCSDT(Q) potentials is converged to better than 0.1 cm^{-1}. We also devised a method by which to investigate the sensitivity of the resonances to changes in the PESs; using an *S*-matrix Kohn variational method (*36*, *37*), we isolated a square integrable resonance contribution to the wave function, which allowed us to compute the first-order response to changes in the PES as a simple integral. We tested overall scaling, scaling of the correlation energy alone, the anisotropy of the PESs, or a radial shift (supplementary materials). We found that in all cases, all resonances shift in the same direction by nearly the same amount of energy, implying that it is hard to adjust the position of the highest resonance into closer agreement with the experiment without affecting the lower-lying resonances, even if we admit much larger variations than the expected uncertainty of the potential. With uncertainties in the PESs virtually ruled out as a non-negligible source of error in the resonance positions, we performed three further checks: We investigated (i) the effect of including scalar relativistic effects, (ii) the effect of explicitly including NO zero-point vibrational motion, and (iii) the effect of the diagonal Born-Oppenheimer correction (DBOC). This last test required a modification of the usual DBOC because the two-PESs scattering method already corrected for the dominant non–Born-Oppenheimer couplings. These three checks are discussed in detail in the supplementary materials, and all three were found to have a negligible effect.

We analyzed the partial-wave composition of the resonances from the CCSDT(Q) potentials and expressed them in terms of the total angular momentum with conserved quantum number $\mathcal{J}$, which forms from the coupling of the rotational state of NO with quantum number $j = 0.5$ and the partial-wave quantum numbers ℓ_{in} and ℓ_{out} that represent the relevant partial waves in the ingoing and outgoing channel, respectively: $\mathcal{J} = \ell_{in/out} \pm 0.5$ (Fig. 1B). Each observed resonance feature was found to consist of a set of overlapping resonances, which we could characterize as mostly pure Feshbach resonances (supplementary materials), with a distinctive value for the resonant partial wave ℓ_{res} corresponding to the quasi-bound NO-He state from which the resonance originates. The resonance below 1 cm^{-1} is characterized by the lowest possible value for $\mathcal{J}$ and ℓ_{res} ($\mathcal{J} = 0.5$; $\ell_{res} = 2$), corresponding to the

lowest NO-He quasi-bound state located just above the energetic asymptote of the free NO radical and He atom. Resonances with $\ell_{res} = 0$ or 1 do not exist because these values correspond to real bound states supported by the potential well (fig. S9 and table S4). The $\ell_{res} = 2$ resonance is further characterized by almost equal contributions of outgoing waves, with $\ell_{out} = 0$ (*s*-wave) and $\ell_{out} = 1$ (*p*-wave). From the ICS calculated in an extended energy regime [Fig. 2; the results based on the CCSD(T) potentials are provided in fig. S8], this resonance was found to connect to the pure *s*-wave Wigner regime, where the ICS is proportional to $1/\sqrt{E}$. The series of resonance features found at higher energies follow the progression of $\ell_{res} = 2, 3, 4, 5, \ldots$ and probe the consecutive series of quasi-bound NO-He states supported by the interaction potential.

The underlying partial-wave composition of a resonance was directly reflected in the energy dependence of the DCS. We first analyzed the inherent structure of the DCS by compiling a contour plot of the theoretically predicted DCS versus collision energy (Fig. 1C). We found that at energies in between the resonances, the DCS was rather independent of the collision energy. By contrast, at a resonance, the DCS was observed to change rapidly, following the rapid change of contributing partial waves. At the resonance energies, it was possible to discern the two dominant ingoing and outgoing partial waves ℓ_{in} and ℓ_{out} underlying the resonance from the DCS: The number of nodes observed in the angular distribution equals the highest value of ℓ.

We experimentally probed the energy dependence of the DCS by measuring scattering images at selected energies at which the DCS was predicted to change rapidly with collision energy and compared them with a simulated scattering image based on the CCSDT(Q) potentials and kinematics of the experiment (Fig. 3). At the lowest energies probed, the velocity images were small, but we could still discern structure in the images. For energies up to 0.7 cm^{-1}, we found strong backscattering, which evolved into a forward-backward peaked structure at energies around 0.7 to 0.8 cm^{-1}. The observed distributions arose from the interference of the *s*- and *p*-waves that dominate the scattering at these low energies. For energies greater than 0.8 cm^{-1}, we observed a rich energy dependence of the DCS, with additional peaks and nodes appearing, reflecting the addition of consecutive partial waves as the energy was increased. We extracted angular scattering distributions from the experimental and simulated images and found excellent agreement with the experimental and simulated distributions.

The resonance structures in both the ICS and DCS as reported here were extremely sensitive to the details of the PESs: The small change in well-depth between the CCSD(T) and CCSDT(Q) PESs caused an experimentally observable shift in resonance position. We investigated this sensitivity further by measuring the resonance position found around 1.3 cm^{-1} for collisions of He with ^{14}NO and ^{15}NO (Fig. 4). The isotope effect and associated change in reduced mass, center-of-mass point of the NO-He complex, and rotational constant resulted in a difference in the centrifugal barrier, anisotropy of the potential, and change in energies of the rotational states (fig. S13). Consequently, the resonance position for He collisions with the heavier ^{15}NO radical was found to shift by ~0.18 cm^{-1} to lower energies, primarily caused by a change in the rotational constant and in excellent agreement with theoretical predictions.

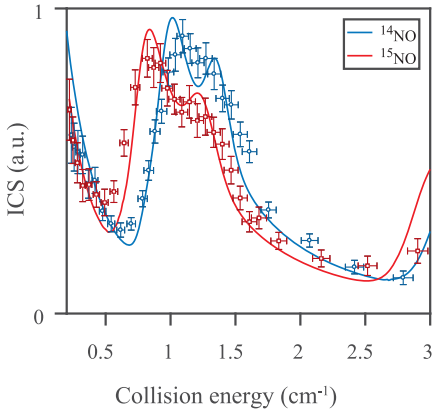

Fig. 4. Measurements of the relative state-to-state ICSs for inelastic ($j = 0.5f \rightarrow j = 0.5e$) collisions of $^{14}N^{16}O$ and $^{15}N^{16}O$ with He around the resonance feature at 1 cm^{-1}. Blue data points indicate $^{14}N^{16}O$, and red data points indicate $^{15}N^{16}O$. Shown also are the calculated cross sections from the CCSDT(Q) potential convoluted with the experimental resolution. Vertical error bars represent statistical uncertainties at 95% CI. Horizontal error bars represent uncertainties in energy calibration.

Our joint experimental and theoretical studies of partial-wave resonances for the benchmark NO-He system at energies down to 0.2 cm^{-1} showed that cold collisions in chemically relevant systems can be probed with full quantum-state resolution—at the partial-wave level—and at energies approaching the Wigner regime. Measurements of the collision energy dependence of the ICS and, in particular, the DCSs revealed how molecular collisions transformed from ultracold into hot by subsequently adding a partial wave as the energy is increased, bridging the gap between the ultracold quantum physics and physical chemistry communities. The high resolution with which resonances were probed experimentally required theory beyond the gold-standard CCSD(T) level to obtain quantitative agreement and allowed for the observation of minute isotope shifts in the resonance positions. The energies attained here were lower than the typical interaction energy of a molecule that posseses an electric or magnetic dipole moment with an external electric or magnetic field, respectively, opening up the possibility to tune the collision dynamics with tailored electric or magnetic fields, maintaining the quantum-state preparation of the reagents and the quantum-state resolution of the products. Field control of cold molecular collisions would transform these studies from merely probing nature with the highest possible level of detail into manipulating nature with the highest possible level of control.

REFERENCES AND NOTES

1. R. D. Levine, R. B. Bernstein, *Molecular Reaction Dynamics and Chemical Reactivity* (Oxford Univ. Press, 1987).
2. A. Schiffman, D. W. Chandler, *Int. Rev. Phys. Chem.* **14**, 371–420 (1995).
3. M. Brouard, C. Vallance, *Tutorials in Molecular Reaction Dynamics* (RSC Publishing, 2010).
4. M. McDonald *et al*., *Nature* **535**, 122–126 (2016).
5. W. E. Perreault, N. Mukherjee, R. N. Zare, *Science* **358**, 356–359 (2017).
6. J. L. Bohn, A. M. Rey, J. Ye, *Science* **357**, 1002–1010 (2017).
7. R. Krems, W. Stwalley, B. Friedrich, Eds., *Cold Molecules: Theory, Experiment, Applications* (Taylor and Francis, 2009).
8. E. P. Wigner, *Phys. Rev.* **73**, 1002–1009 (1948).
9. M. T. Bell, T. P. Softley, *Mol. Phys.* **107**, 99–132 (2009).
10. W. Erlewein, M. von Seggern, J. P. Toennies, *Z. Phys.* **211**, 35–50 (1968).
11. C. Naulin, M. Costes, *Int. Rev. Phys. Chem.* **33**, 427–446 (2014).
12. W. Dong *et al*., *Science* **327**, 1501–1502 (2010).
13. T. Yang *et al*., *Science* **347**, 60–63 (2015).
14. J. B. Kim *et al*., *Science* **349**, 510–513 (2015).
15. D. Hauser *et al*., *Nat. Phys.* **11**, 467–470 (2015).
16. J. Weiner, V. S. Bagnato, S. Zilio, P. S. Julienne, *Rev. Mod. Phys.* **71**, 1–85 (1999).
17. G. Quéméner, P. S. Julienne, *Chem. Rev.* **112**, 4949–5011 (2012).
18. J. Jankunas, A. Osterwalder, *Annu. Rev. Phys. Chem.* **66**, 241–262 (2015).
19. S. Chefdeville *et al*., *Phys. Rev. Lett.* **109**, 023201 (2012).
20. M. Lara *et al*., *Phys. Rev. Lett.* **109**, 133201 (2012).
21. S. Chefdeville *et al*., *Science* **341**, 1094–1096 (2013).
22. A. Bergeat, J. Onvlee, C. Naulin, A. van der Avoird, M. Costes, *Nat. Chem.* **7**, 349–353 (2015).
23. A. Bergeat *et al*., *Nat. Chem.* **10**, 519–522 (2018).
24. A. B. Henson, S. Gersten, Y. Shagam, J. Narevicius, E. Narevicius, *Science* **338**, 234–238 (2012).
25. E. Lavert-Ofir *et al*., *Nat. Chem.* **6**, 332–335 (2014).
26. A. Klein *et al*., *Nat. Phys.* **13**, 35–38 (2017).
27. Y. Shagam *et al*., *Nat. Chem.* **7**, 921–926 (2015).
28. J. Jankunas, K. Jachymski, M. Hapka, A. Osterwalder, *J. Chem. Phys.* **142**, 164305 (2015).
29. S. N. Vogels *et al*., *Science* **350**, 787–790 (2015).
30. S. N. Vogels *et al*., *Nat. Chem.* **10**, 435–440 (2018).
31. S. S. Kondov *et al*., *Phys. Rev. Lett.* **121**, 143401 (2018).
32. The labels $X^2\Pi_{1/2}$, *v*, and *j* indicate the electronic state, the vibrational state, and rotational state of the NO radical, respectively. Each rotational state of NO possesses two near-degenerate Λ-doublet components, with symmetry labels *e* (lower component) and *f* (upper component), that refer to the total parity of the electronic wave function, exclusive of rotation.
33. The abbreviations CCSD(T), CCSDT(Q), and CCSDTQ(P) denote the level of coupled-cluster (CC) theory used to calculate potential-energy surfaces, which include single (S), double (D), triple (T), quadruple (Q), and quintuple (P) excitations of electrons. The last letter in parenthesis indicates perturbative treatment of the excitation. The prefix letter U stands for unrestricted and further details the implementation of the theoretical methods.
34. P. Jankowski, A. R. W. McKellar, K. Szalewicz, *Science* **336**, 1147–1150 (2012).

35. W. L. Meerts, A. Dymanus, *J. Mol. Spectrosc.* **44**, 320–346 (1972).
36. J. Z. H. Zhang, W. H. Miller, *J. Chem. Phys.* **91**, 1528–1547 (1989).
37. G. C. Groenenboom, D. T. Colbert, *J. Chem. Phys.* **99**, 9681–9696 (1993).
38. T. de Jongh, M. Besemer, Q. Shuai, T. Karman, A. van der Avoird, G. C. Groenenboom, S. Y. T. van de Meerakker, Imaging the onset of the resonance regime in low-energy NO-He collisions online data. DANS (2020); doi:10.17026/dans-x4h-ur6f.

ACKNOWLEDGMENTS

We thank J. Klos for providing us with NO-He PESs at the CCSD(T) level, T. Cremers for developing data acquisition software, and J. Stanton for help with DBOC calculations. We thank N. Janssen and A. van Roij for expert technical support. **Funding:** This work is part of the research program of the Netherlands Organization for Scientific Research (NWO). S.Y.T.v.d.M. acknowledges support from the European Research Council (ERC) under the European Union's Seventh Framework Program (FP7/2007-2013/ERC grant agreement 335646 MOLBIL) and from the ERC under the European Union's Horizon 2020 Research and Innovation Program (grant agreement 817947 FICOMOL). **Author contributions:** The project was conceived by S.Y.T.v.d.M. The experiments, data analysis, and simulations were carried out by T.d.J. and Q.S. Potential energy surfaces and scattering cross sections were calculated by M.B., A.v.d.A., and G.C.G. DBOC calculations for open-shell systems were performed by G.C.G. The *S*-matrix Kohn-variational method was implemented by T.K. All authors were involved in the interpretation of the data, discussed the results, and commented on the manuscript. The paper was written by T.d.J., M.B., and S.Y.T.v.d.M., with contributions from all authors. **Competing interests:** None declared. **Data and materials availability:** All data are available in the main text or the supplementary materials, as well as online at DANS (*38*).

SUPPLEMENTARY MATERIALS

science.sciencemag.org/content/368/6491/626/suppl/DC1
Supplementary Text
Figs. S1 to S13
Tables S1 to S4
References (*39*–*70*)

29 November 2019; accepted 19 March 2020
10.1126/science.aba3990

Imaging the onset of the resonance regime in low-energy NO-He collisions

Tim de Jongh, Matthieu Besemer, Quan Shuai, Tijs Karman, Ad van der Avoird, Gerrit C. Groenenboom and Sebastiaan Y. T. van de Meerakker

Science **368** (6491), 626-630.
DOI: 10.1126/science.aba3990

Ultracold molecular collision dynamics

Ultracold collision dynamics are of great importance in understanding the quantum nature of chemical interactions, but achieving the ultracold regime for molecules is challenging. Traditional techniques based on alternative routes to assemble the ultracold atomic constituents are only able to produce a type of ultracold molecules that cannot probe state-selective dynamics. Using Stark deceleration and velocity map–imaging techniques, de Jongh *et al.* achieved the ultracold regime directly for a nitric oxide–helium system and measured the state-to-state cross sections for inelastic scattering with high precision (see the Perspective by Yang and Yang). The observed scattering resonances confirmed high sensitivity to the underlying interaction potential because only the most accurate electronic structure theory could reproduce their structure.

Science, this issue p. 626; see also p. 582